Heliyon 9 (2023) e21033

Contents lists available at ScienceDirect

Heliyon

journal homepage: www.cell.com/heliyon

Voltammetric determination of tryptophan at graphitic carbon nitride modified carbon paste electrode

Habtamu Adefris Abebe, Abebe Diro, Shimeles Addisu Kitte *

Department of Chemistry, College of Natural Sciences, Jimma University, P. O. Box 378, Jimma, Ethiopia

ARTICLE INFO

Keywords:
Electrochemical detection
Tryptophan
Graphitic carbon nitride modified carbon paste electrode
Cyclic voltammetry
Linear sweep voltammetry

ABSTRACT

Herein, we reported carbon paste electrode modified with graphitic carbon nitride (g–C_3N_4–CPE) to determine of tryptophan (Trp) using voltametric techniques. Various spectroscopic and electrochemical techniques were used to characterize the as-synthesized g-C_3N_4 and the assembled electrodes. The transfer coefficient, rate constant and the diffusion coefficient of Trp in this system were found to be 0.28, $1.9 \times 10^4\ M^{-1}s^{-1}$ and $3.2 \times 10^{-5}\ cm^2s^{-1}$, respectively. The linear range was obtained for the detection of Trp using LSV is from 0.1 μM to 120 μM at pH 5. The limit of detection (LOD) ($3\sigma/m$) was 0.085 μM. The demonstrated modified CPE was also effectively used for the detection of Trp in milk with percentage recovery of 98 %–105.2 %. Furthermore, the modified CPE exhibited good repeatability, reproducibility and appropriate selectivity.

1. Introduction

Tryptophan (Trp) is an essential amino acid with biochemical, nutritional, and medical significance in humans [1]. It is useful for various important issues, such as for nitrogen balance in human development, production of niacin, which is very essential for secretion of serotonin and melatonin neurotransmitters [2,3]. Insufficient amount of Trp in human body results in less amount of these neurotransmitters thus, sleep disorders and depression may be occurred [4,5]. Hence, it is of great importance to develop accurate and economical method to detect Trp in pharmaceutical, food products and biological samples.

Until now, numerous analytical detection methods have been established for the Trp sensing such as chromatography [6], chemiluminescence [7], capillary electrophoresis [8], spectroscopic detection [9]. As Trp is electroactive, electrochemical methods with high sensitivity, selectivity, fast response and easy operation gained more attention. However, it is still difficult to measure Trp directly at unmodified electrodes due to the slowness of the redox process leads to high overpotential at the electrode [10,11].

Carbon nitrides are a type of polymeric substances primarily made up of carbon and nitrogen. One of the carbon nitride allotropes with interesting characteristics is graphitic carbon nitride (g-C_3N_4), which has a high surface area and superior electrocatalytic activity. In addition, its high thermal and chemical stability allows it to function well in various chemical environments and at high temperatures [12,13]. g-C_3N_4 has been widely utilized for a variety of sensing applications. g-C_3N_4 nano-sheet modified carbon paste electrode (CPE) for methotrexate sensing was recently described by Saleh et al. [14]. Balasubramanian and co-workers successful synthesized and used g-C_3N_4 for voltammetric determination the antibiotic sulfamethoxazole [15]. A rapid voltammetric sensor for the detection of sulfathiazole and sulfapyridine was demonstrated by Javad et al. using CPE modified with g-C_3N_4 and manganese oxide [16]. Ilager and his co-workers developed cetyltrimethylammonium bromide and g-C_3N_4 modified CPE to determine trace amounts of

* Corresponding author.
E-mail address: shimeles.addisu@ju.edu.et (S.A. Kitte).

https://doi.org/10.1016/j.heliyon.2023.e21033
Received 8 June 2023; Received in revised form 30 September 2023; Accepted 13 October 2023
Available online 14 October 2023

the herbicides [17].

Adams was the first to introduce the carbon paste electrode (CPE), one of the widely used electrodes [18]. CPEs are made up of graphite powder and liquid binder assembled into a properly prepared electrode body [19]. Due to its unique features, such as low cost, superior electrical characteristics, large potential windows, and easy surface renewability, CPEs have been used extensively as voltametric transducers for the determination of important electroactive substances [20–22]. Other than the interesting properties listed before, the possibility of modification of CPE by incorporating various substances during preparation has become widely employed to enhance electron transfer process for sensitive determination of electroactive species [23]. For instance modified CPEs have been commonly used for sensitive analysis of trace heavy metals [24,25], biologically important substances [26], drugs [27], food [28] and so on. In this paper, we showed how to easily create a g–C_3N_4–CPE for sensitive electrochemical detection for Trp. In comparison to bare CPE, the g–C_3N_4–CPE showed superior electrochemical catalytic characteristics, less overpotential and increased anodic peak current of Trp. Furthermore, the suggested electrode showed excellent repeatability, reproducibility, and a suitable detection limit. Trp in a milk sample was successfully determined using the produced g–C_3N_4–CPE. The approach used in this study can also be used to other electroactive compounds.

2. Materials and methods

2.1. Chemicals

Trp ($C_{11}H_{12}N_2O_2$, 99.9 %) (Sinopharm Chemical Reagent, China), urea (CH_4N_2O, 99 % (Alfa Aesar Chemical Reagent, China), phosphoric acid (H_3PO_4, 85 %, (Riedel de Haen, Germany), sodium hydroxide (NaOH, 98 %, Loba Chemie, India), potassium chloride (KCl, 99.8 %) (Aladdin Reagents, China), graphite powder (98 %) (BDH, England), potassium dihydrogen phosphate (KH_2PO_4, 99.5 %) (Aladdin Reagents, China), Potassium phosphate dibasic (K_2HPO_4, 99 %) (Aladdin Reagents, China), paraffin oil (light, density : 0.84–0.86) (Aladdin Reagents, China) were used. All the aqueous solutions were prepared with double distilled water.

2.2. Instrumentations

The surface structure of the prepared g-C_3N_4 was examined using scanning electron microscopy (JCM-6000 plus). The X-ray diffraction (XRD) (XPERT-PRO, The Netherlands) spectroscopy was used to depict the crystal structure of g-C_3N_4. Fourier transform infrared spectroscopy (FT-IR) (JASCO 4600LE spectrometer) was used to analyze the functional groups. Epsilon (Bioanalytical System, USA) was used for investigate CV and LSV experiments. As a working, reference, and auxiliary electrode, respectively, we used g–C_3N_4–CPE, Ag/AgCl (saturated KCl), and platinum wire.

2.3. Preparation of g-C_3N_4

In a muffle furnace, 10 g of urea was heated to 450 °C, 500 °C, 550 °C, and 600 °C at a rate of 5 °C min^{-1} and kept at each temperature for 2 h under air conditions. Yellow-colored g-C_3N_4 was found after cooling to room temperature. Then, it was crushed and preserved until used [29].

2.4. Sample preparation

10 mM Trp was prepared as a stock solution using double distilled water and working solution of Trp was prepared by diluting a required volume of stock solution of Trp in 0.1 M PBS of pH 5.0 at the day of the experiment. As a supporting electrolyte, 0.1 M phosphate buffer solutions (PBS), pH 5.0, were prepared using 0.1 M KH_2PO_4 and Na_2HPO_4.

2.5. Preparation of bare CPE

To prepare CPE, paraffin oil (20 % (w/w)) and graphite powder (80 % (w/w)) were homogenized in a mortar and pestle for 1 h. A Teflon tube (3 mm in diameter) was filled with the resulting paste. At the opposite end of the Teflon tube copper wire was inserted for electrical contact. Finally, a clean, smooth sheet of weighing paper was used to smooth the surface of the assembled CPE.

Table 1
The Compositions of g–C_3N_4–CPE tested.

No	Composition (%w/w)		
	g-C_3N_4	Graphite powder	Paraffin oil
1	10	70	20
2	15	65	20
3	20	60	20
4	25	55	20
5	30	50	20
6	35	45	20

2.6. Preparation of g–C_3N_4–CPE

The g–C_3N_4–CPE was prepared by mixing various compositions of g-C_3N_4 and graphite powder as shown in Table 1. The graphite powder, g-C_3N_4 and paraffin liquid were mixed uniformly for 1 h. Then the homogenized paste was filled in a Teflon tube in the same manner as unmodified CPE was prepared.

2.7. Real sample analysis

For real samples analysis, the percentage recoveries were done by spiking different standard solution of Trp. Fresh milk was obtained from a market, in Jimma, Ethiopia. Firstly, 1 mL of 0.01 M HCl was mixed with 5.0 mL of the purchased milk and agitated for 10 min [30]. Then, the supernatant was taken after the resulting solution was centrifuged for 20 min at 8000 rpm. Then, Trp was detected to prove the capability of the proposed modified CPE to sense Trp in milk sample. Determination of Trp in milk samples was taken place under the optimum experimental conditions.

3. Results and discussion

3.1. Characterization of g-C_3N_4

Fig. 1A shows the results of the XRD analysis of the crystal structure of the prepared g-C_3N_4. The polymerization temperatures used to produce the g-C_3N_4 ranged from 450 to 600 °C. Two distinct peaks in the XDR pattern, at 13.2° and 27.6°, respectively, are attributed to the planes of the (100) and (002) crystal planes of g-C_3N_4 (JPCDS No. 87–1526) [31]. The (002) reflection of an aromatic graphitic structure is responsible for the high peak found at 27.6°, and a weak diffraction peak at 13.2° is due to the heptazine network [32].

Fig. 1B, displays the FT-IR spectra of the g-C_3N_4 synthesized at different polymerization temperatures. The absorption peak at 810 cm^{-1} denotes the formation of g-C_3N_4 with triazine or heptazine rings. The peak between 1200 and 1650 cm^{-1} are given to the typical

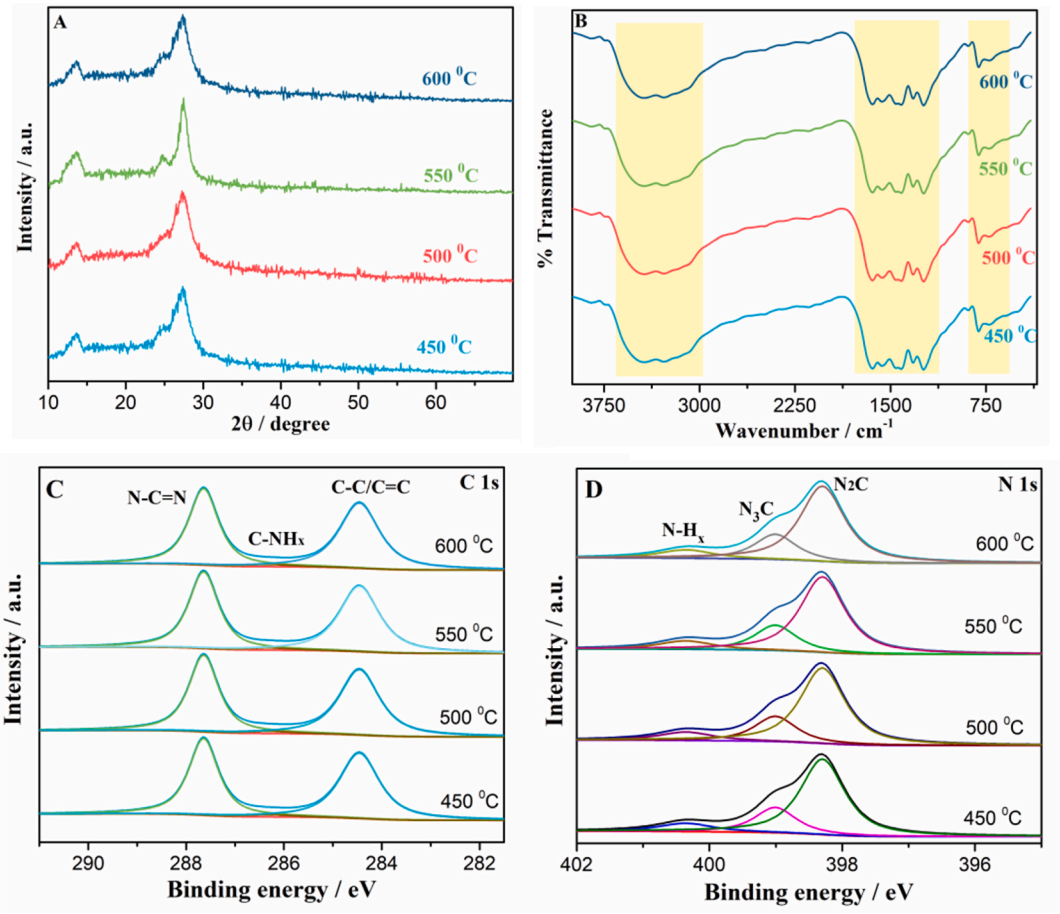

Fig. 1. XRD patterns (A), FT-IR spectra (B), C 1s (C) and N 1s (D) XPS spectra of *g*-C_3N_4 synthesized at different temperatures.

stretching modes of carbon nitride heterocycles [33], the peak seen in the region of 3000–3500 cm^{-1} was due to N–H stretchings [34].

The chemical states of nitrogen and carbon in the synthesized g-C_3N_4 were also examined using XPS. The C 1s spectra of the g-C_3N_4 produced at 450, 500, 550, and 600 °C are shown in Fig. 1C. The peaks identified as C–C/C–C, C-NHx, and N–C–N at 284.7, 286.5, and 288.7 eV, respectively. The N 1s spectra for g-C_3N_4 at different temperatures were obtained at approximately 398.7, 399.9, and 400.9 eV (Fig. 1D), and they can be referred to the N–C–N ($N(C)_2$), N–C–N ($N(C)_3$), and N-Hx bonds, respectively [35,36].

Using the SEM technique, the surface morphology of the g-C_3N_4 was examined. SEM images show the prepared g-C_3N_4 are composed of loaded layered structure (Fig. 2A–D) [37].

3.2. CV and EIS characterization of bare CPE and g–C_3N_4–CPE

Using CV and EIS, the electrical response of bare and modified CPE was studied in 0.1 mM $[Fe(CN)_6]^{3-/4-}$ containing 0.1 M KCl. Both bare CPE and g–C_3N_4–CPE exhibited a pair of redox peaks, as shown in Fig. 3A. However, compared to bare CPE, g–C_3N_4–CPE displayed stronger redox peak currents. This is because g-C_3N_4 enhanced the conductivity of the modified CPE which enables rapid transfer of electron at the electrode-solution interface [38]. EIS is also a vital tool for analyzing the interfacial electrochemical behavior of electrodes [39]. For the purpose of evaluating the impedance of the bare CPE and g–C_3N_4–CPE, EIS experiments were conducted in $[Fe(CN)_6]^{3-/4-}$ solution. The charge transfer resistance (R_{ct}) at the electrode surface correlates to the diameter of the semicircle in the Nyquist plot. As shown in Fig. 3B, g–C_3N_4–CPE (curve *b*) exhibits a smaller semicircle than bare CPE (curve *a*), corresponding to a lower R_{ct} which is consistent with the CV results.

For the purpose of determining electrochemical active surface area (EASA), the CVs were measured in $[Fe(CN)_6]^{3-/4-}$ solution at different scan rates (10–100 mV/s) on both bare CPE and g–C_3N_4–CPE (Fig. 3C). Using the Randles-Sevcik equation, the EASA of the electrode was calculated. The following equation (Eq. (1)) describes the peak current (I_p) [40].

$$I_p = 2.69 \times 10^5 n^{3/2} A D^{1/2} v^{1/2} C \ldots\ldots\ldots\ldots\ldots \quad (1)$$

where n denotes the electron number (1 for $[Fe(CN)_6]^{3-}$), A denotes the surface area, D denotes the diffusion coefficient (7.6×10^{-6} cm^2s^{-1}), C is the $[Fe(CN)_6]^{3-}$concentration (1×10^{-4} $molcm^{-3}$) and v denotes the scan rate (Vs^{-1}). The EASA of bare CPE and g–C_3N_4–CPE was found to be 0.34 and 0.72 cm^2, respectively.

3.3. Cyclic voltammetric study of Trp at bare CPE and g–C_3N_4–CPE

Fig. 3D shows the voltammograms of bare CPE and g–C_3N_4–CPE in the blank PBS and in the presence of Trp. In blank PBS, both bare CPE and g–C_3N_4–CPE (curves *a* and *b*) shows no redox peaks. In 10 μM Trp solution, both electrodes showed anodic peaks (curves *c* and *d*). No cathodic peaks were observed for Trp in backward scan, thus confirming the redox process of Trp is irreversible at bare CPE and g–C_3N_4–CPE. Furthermore, the oxidation peak for Trp was observed at an anodic peak potential (E_{pa}) of 1.06 V for bare CPE with a anodic peak current (I_{pa}) value of 39.1 μA (curve *c*). For g–C_3N_4–CPE the E_{pa} was observed at 1.02 V and I_{pa} of 268 μA (curve *d*). The higher oxidation peak current at g–C_3N_4–CPE is ascribed to the higher efficiency of electron transfer due to the presence of g-C_3N_4.

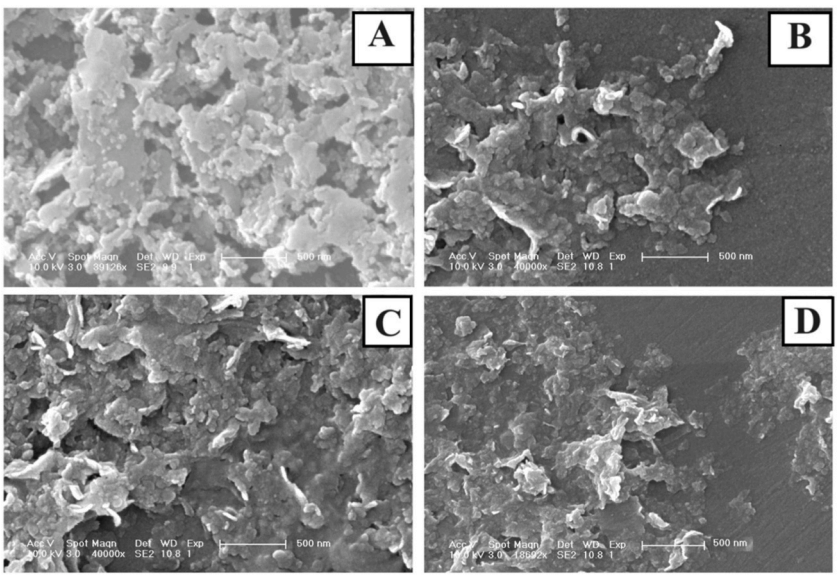

Fig. 2. Images taken using SEM for g-C_3N_4 at 450 °C (A), 500 °C (B), 550 °C (C), and 600 °C (D).

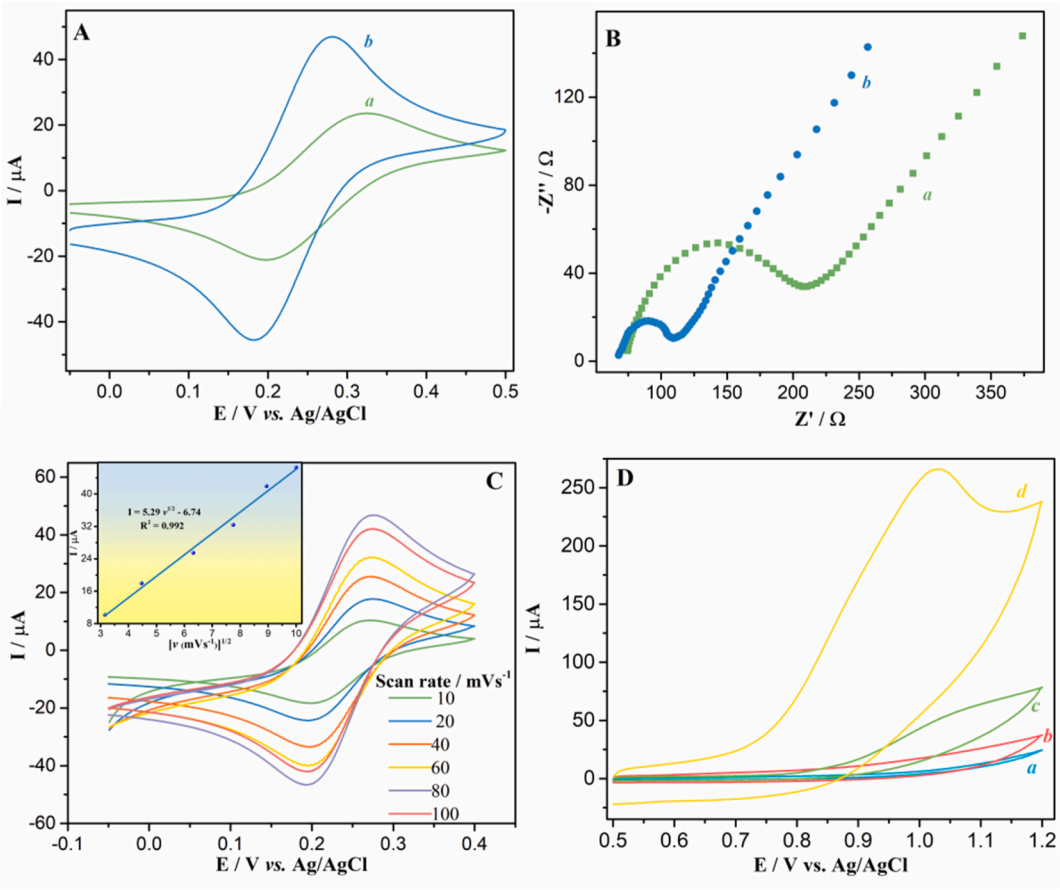

Fig. 3. (A) CVs and (B) the Impedance spectra ((*a*) bare CPE and (*b*) g–C_3N_4–CPE) in 0.1 M KCl containing 0.1 mM $[Fe(CN)_6]^{3-/4-}$; (C) CVs of the g–C_3N_4–CPE in $[Fe(CN)_6]^{3-}$ at different scan rates for EASA calculation (The inset: *I vs.* $\nu^{1/2}$ plot); (D) CVs of bare CPE in blank (*a*) & in 10 µM Trp (*c*) and g–C_3N_4–CPE in blank (*b*) & in 10 µM Trp (*d*) in 0.1 M pH 5.0 PBS at 100 mV/s scan rate.

3.4. *Effects of pH*

As illustrated in Fig. 4, the pH of buffer on the anodic process of Trp at g–C_3N_4–CPE was examined by recording CVs of Trp in the range from 3.0 to 8.0 (0.1 M PBS). It is clearly seen that the anodic peak currents were changed with the change in the pH of buffer and highest anodic current for Trp was obtained at pH 5.0 (Fig. 4 A and B). Thus, PBS with pH 5.0 was chosen as optimum pH for detection

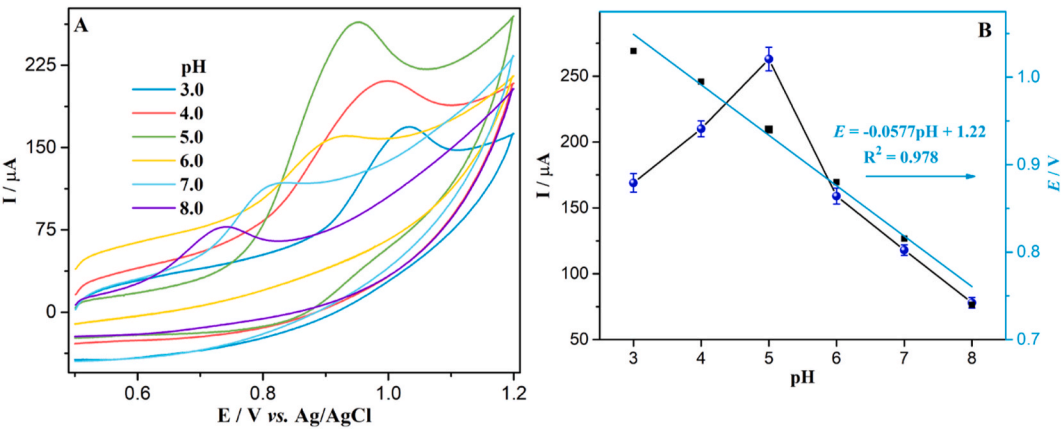

Fig. 4. (A) Effect of pH on anodic process of 10 µM Trp at g–C_3N_4–CPE (B) Plot of oxidation current and potential of Trp as a function of pH.

of Trp in this work. Moreover, the oxidation potential was also affected by a change in pH. The anodic potential of Trp was shifted to a lower potential with rise in pH. This confirms the involvement of the proton in the anodic process. The oxidation potential of Trp is nearly directly related to pH with an equation of E(V) = −0.0577 pH + 1.22, R^2 = 0.978 (Fig. 4B). The acquired slope value was then applied to the Nernst Eq. (2) [41].

$$E_p = \frac{-0.0591\ m}{n} pH + b \quad (2)$$

where, n is the number of electron and m is the number of proton. Using Eq. (2) the value of m/n for Trp was found to be 0.976. This value suggests that the oxidation reaction of Trp at g–C_3N_4–CPE involves an identical number of protons and electrons. Scheme 1 illustrates the Trp oxidation mechanism at g–C_3N_4–CPE. Based on the obtained data, the anodic process of Trp at the g–C_3N_4–CPE was irreversible, two protons and two electrons reaction takes place at the amine in the indole ring and methyl in the side chain.

3.5. Effects of scan rate

The electrode process of Trp at g–C_3N_4–CPE was explored by studying the relation between oxidation current and scan rate. The effect of scan rate on the anodic peak current of Trp at g–C_3N_4–CPE is shown in Fig. 5. The anodic peak currents (I_{pa}) increased when the scan rate increased from 10 to 200 mV/s (Fig. 5A). As shown in Fig. 5B and C, the values of peak current are linearly related with the scan rates (with a regression equation I_{pa} (μA) = 2.71v + 28.9 (R^2 = 0.991)) than the square root of scan rates (with a regression equation I_{pa} (μA) = 35.97v^2 – 63 (R^2 = 0.942). This shows that the anodic reaction of Trp at the g–C_3N_4–CPE is an adsorption-controlled process. Fig. 5D displays a Tafel plot that was obtained using data from the Tafel region of the CV and detail information regarding the rate-determining step was obtained. The points of the Tafel region of the CV of Trp solution at the g–C_3N_4–CPE surface yield a 0.28 electron transfer coefficient (α), assuming that Trp undergo one electron transfer during the rate-determining phase [42].

3.6. Reaction kinetics for oxidation of Trp at g–C_3N_4–CPE

Chronoamperometry (CA) was employed to study the reaction kinetics of the g–C_3N_4–CPE system. Fig. 6 shows the CA response of the g–C_3N_4–CPE in blank and Trp solution in 0.1 M PBS (pH 5.0) at 1.2 V. The CA current response of Trp at g–C_3N_4–CPE (I_p) is significantly greater than the current response g–C_3N_4–CPE in blank (I_b). The kinetic rate constant (K_{cat}) can be calculated using Eq. (3) [43,44]:

$$\frac{I_p}{I_b} = (\pi KCt)^{1/2} \quad (3)$$

where I_p is current response of g–C_3N_4–CPE in Trp and I_b the current response g–C_3N_4–CPE in blank, C is the concentration of Trp (mol cm^{-3}), t is time (seconds), and reaction rate constant is represented as K. Accordingly, the value of K_{cat} is calculated as 1.9×10^4 $M^{-1}s^{-1}$ from the I_p/I_b *vs.* $t^{1/2}$ plot presented in Fig. 6 (inset). Furthermore, the Cottrell equation can be used to compute the diffusion coefficient (D) of Trp (Eq. (4)) [43,44]:

$$I_p = \frac{nFAC\sqrt{D}}{\sqrt{\pi t}} \quad (4)$$

I_p stands for peak current (A), n for the number of electrons, F for the Faraday constant (96,500C mol^{-1}), A for the electrode's surface area (cm^2), C for the analyte's bulk concentration (mol cm^{-3}), and t for the time (seconds). As a result, using Eq. (4), Trp has a value of $D = 3.2 \times 10^{-5}$ cm^2s^{-1}.

3.7. Effects of modifier composition

By varying the amounts of g-C_3N_4, paraffin oil, and graphite powder, the effect of g-C_3N_4 on the voltammetric response of Trp was investigated. As presented in Fig. 7A, the anodic current rises with increasing the amount of g-C_3N_4 from 10 % up to 30 % (w/w). Higher than 30 % (w/w) of g-C_3N_4 the peak currents decline considerably. This may be due to fewer amounts of graphite powder in the paste and thus decrease in the conductivity of the modified electrode. Therefore, 30 %, 50 % and 20 % (w/w) of g-C_3N_4, graphite powder and paraffin oil, respectively was chosen as the best composition for the modified CPE preparation.

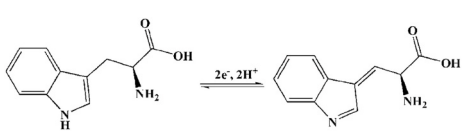

Scheme 1. Anodic reaction mechanism of Trp at g–C_3N_4–CPE.

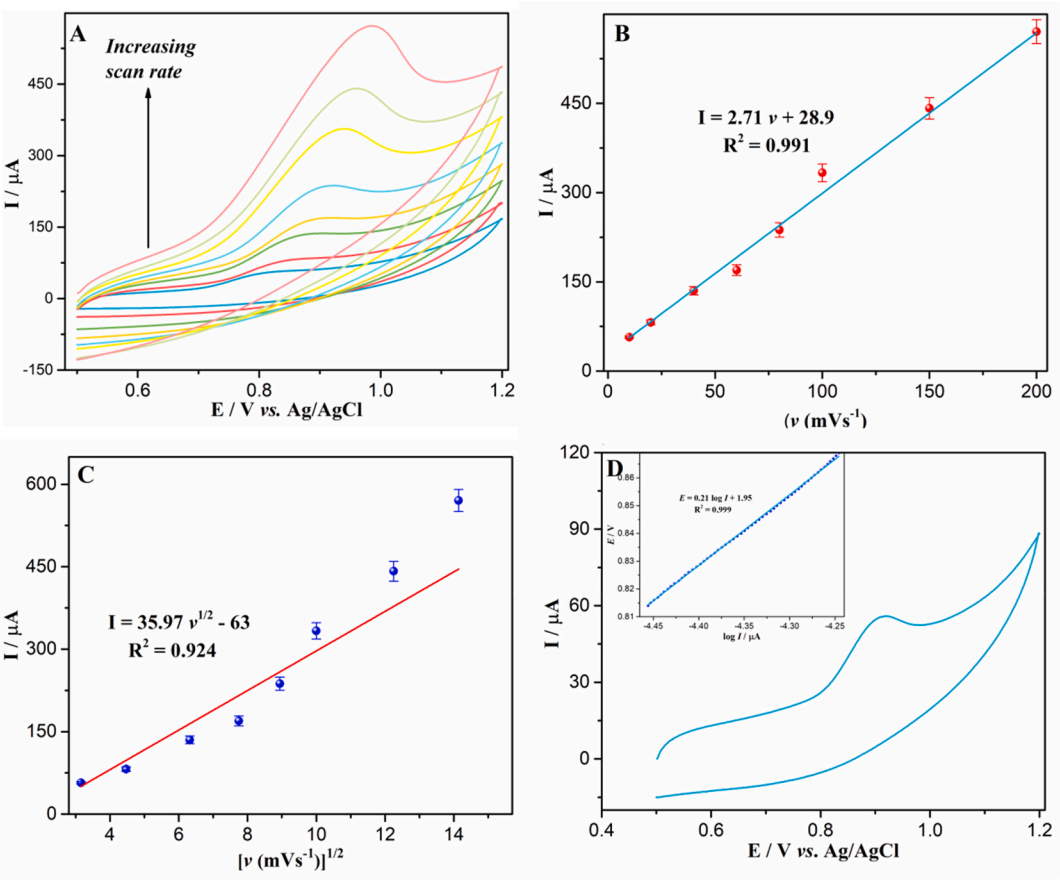

Fig. 5. (A) CVs for Trp in PBS (pH = 5.0) at g–C_3N_4–CPE with different scan rates: 10 to 200 mVs^{-1}; (B) and (C) the plots of the linear relationship between *I vs. v* and *I vs.* $v^{1/2}$; (D) CV of 10 µM Trp at 10 mVs^{-1} scan rate in 0.1 M PBS (pH 5.0) used for the Tafel plot (Inset: The Tafel plot).

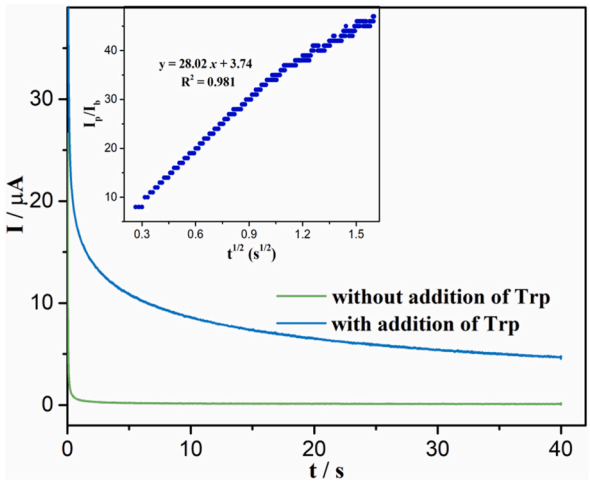

Fig. 6. CA response of g–C_3N_4–CPE in blank and in the presence of Trp in 0.1 M PBS pH 5 (Inset: plot of I_p/I_b *vs.* $t^{1/2}$).

3.8. Effect of temperature

The dependency of the oxidation current of Trp on the temperature at which the g-C_3N_4 was synthesized was examined. By raising the polymerization temperature up to 550 °C the oxidation current of Trp was improved, but, the anodic current decreased when the

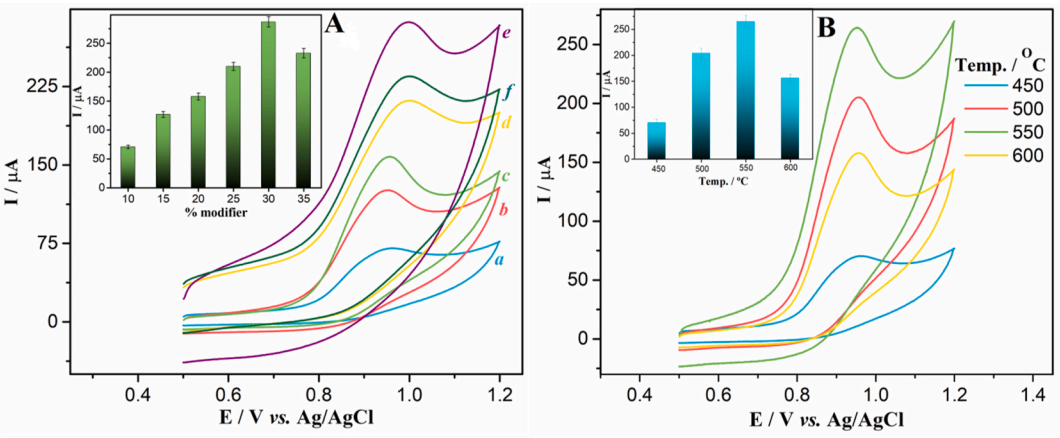

Fig. 7. (A) CVs showing effect of composition of g-C_3N_4 (*a*) 10 %, (*b*) 15 %, (*c*) 20 % (*d*) 25 %, (*e*) 30 %, and (*f*) 35 % on the oxidation current of Trp (Inset of Fig. 6A: Bar graph); (B) CVs showing effect of polymerization temperature of g-C_3N_4 (Inset of Fig. 6B: bar graph).

temperature increases to 600 °C (Fig. 7B). Therefore, polymerization temperature of 550 °C was selected as an optimum temperature.

3.9. Calibration plot of Trp

Fig. 8 shows LSVs of different concentration of Trp at g–C_3N_4–CPE recorded at optimal experimental parameters. The anodic current of Trp was rises with increasing the concentration of Trp (Fig. 8A). The anodic current of Trp at g–C_3N_4–CPE is directly related to the Trp concentration in the range of 0.1 µM–120 µM (Fig. 8B), with regression equation:

$$I(\mu A) = 5.04\ C(\mu M) + 4.49, R^2 = 0.998.$$

The calculated limit of detection (LOD) is about 0.085 µM ($3\sigma/m$) where σ is the standard deviation of the blank and m is the slope of the calibration equation. The dynamic linear range, the type of modifier used and LOD of the present work was compared with other related voltammetric techniques reported earlier for the detection of Trp and summarized in Table 2. We can confirm that the g–C_3N_4–CPE attained a comparable linear range, the type of modifier used and LOD with the previously reported electrochemical methods.

3.10. Repeatability and reproducibility

The repeatability of g–C_3N_4–CPE was obtained by recording the oxidation current values for 10 µM Trp for 9 repeated measurements, thus, the RSD was obtained at 1.9 % (Fig. 9A). CA study was also checked for long time with presence and absence of Trp for the stability test and shows good stability (Inset of Fig. 9A). For reproducibility test, three different g–C_3N_4–CPEs, which were assembled separately by following the same assembly procedure were tested and RSD of 5.6 % for the determination of 10 µM Trp was attained (Fig. 9B). Therefore, we can conclude that acceptable repeatability and reproducibility was obtained for the determination of Trp at g–C_3N_4–CPE. Furthermore, the stability of the anodic current response of 10 µM Trp was tested at g–C_3N_4–CPE after the electrode was reserved at room temperature for one month. The observed result indicates that 92.5 % of the initial oxidation current value was obtained, signifying excellent stability.

3.11. Real sample analysis

The practical use of the demonstrated modified CPE for the sensing Trp was applied to detect Trp in milk sample by spiking a standard Trp (5, 10, 20 and 30 µM) and the %recovery was calculated. As summarized in Table 3, the recovery values of Trp in the milk sample were obtained from 98 % to 105.2 %.

3.12. Interference study

To evaluate the effect of selected interfering substances such as, ascorbic acid (AA), dopamine (DA), uric acid (UA), L-cysteine (L-cys), L-arginine (L-arg), L-alanine (L-ala), and methionine (Meth) were used as depicted in Fig. 10. It was found that 10 fold higher concentrations of the selected biological substances did not interfere in the analysis of Trp. This might be because the different redox potentials of the selected substances. Thus demonstrated modified CPE has outstanding selectivity towards Trp.

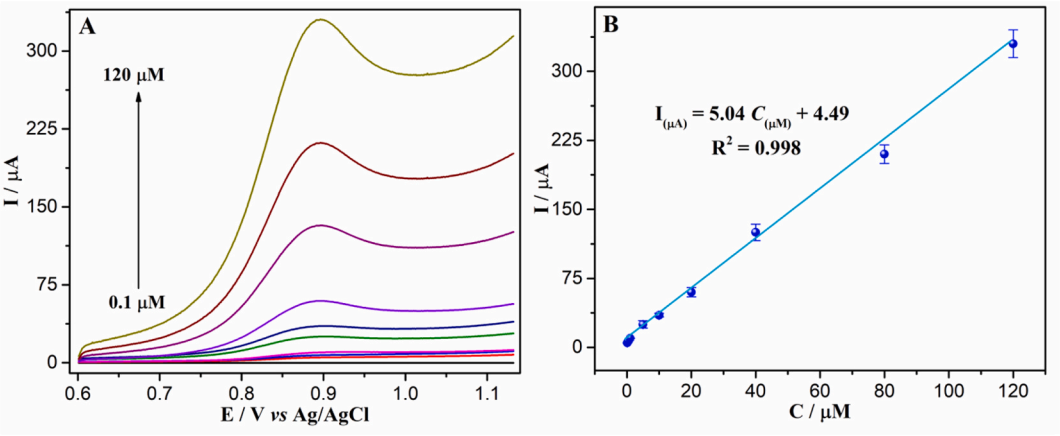

Fig. 8. (A) The LSV response for different concentration of Trp at g–C_3N_4–CPE; (B) Plot of linear calibration curve of Trp at g–C_3N_4–CPE at a pH of 5.0.

Table 2
Comparison of the LOD and the linear range of Trp determined at various electrodes.

Electrode	LOD (μM)	Linear range (μM)	Method	Ref.
Poly(glycine) modified carbon nanotube paste electrode	0.42	20–100	DPV	[45]
Nitrogen-doped ordered mesoporous carbon/GCE	0.035	0.5–70 & 70–200	CV	[46]
Nanoporous carbon/GCE	0.03	1–103	Amperometry	[47]
NiO/carbon nanotube (CNT)/poly(3,4-ethylenedioxythiophene)/GCE	0.21	1–41	DPV	[48]
Polyvinylpyrrolidone coated gold nanoparticles modified GCE	0.3	1–50 & 50–350	LSV	[49]
Co_3O_4 nanosheets/rGO composites/GCE	0.26	1–800		[50]
Graphite electrode from waste batteries	1.73	5–150	DPV	[51]
Reduced graphene oxide with SnO_2 nanoparticles/GCE	0.04	1–100	DPV	[52]
Graphene-Modified Electrode	0.3	0.1–100	LSV	[53]
g-C_3N_4-CPE	0.085	0.1–120	LSV	This work

SWV - Square wave voltammetry; DPV - Differential wave Voltammetry.

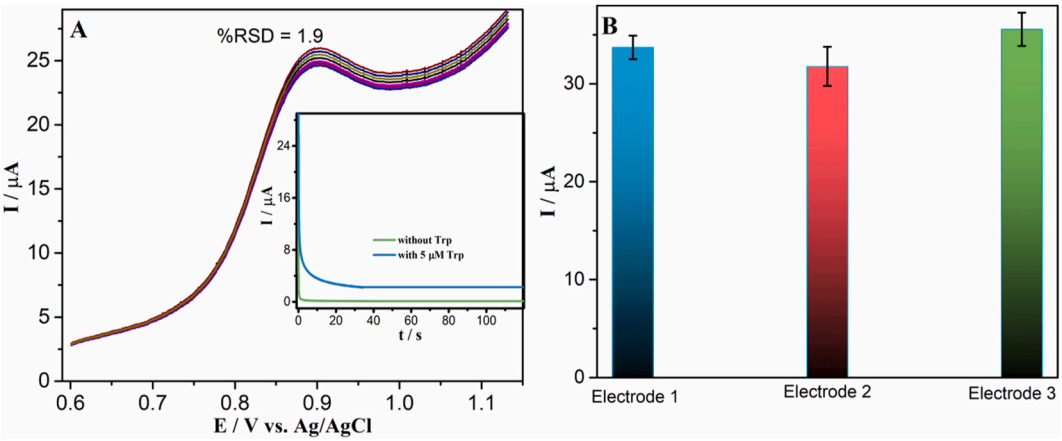

Fig. 9. (A) LSV response nine repeated measurement of 10 μM Trp at g–C_3N_4–CPE (Inset: Chronoamperogram curves of g–C_3N_4–CPE in blank and presence of Trp as stability test); (B) Reproducibility study of the g–C_3N_4–CPE for the detection of 10 μM Trp at three different modified electrodes.

4. Conclusion

In summary, in this work, g–C_3N_4–CPE was proposed and used for the voltammetric detection of Trp. The experimental result showed that g–C_3N_4–CPE was sensitive and its performance is comparable with other CPE based detection of Trp. The modified CPE

Table 3
The application of g–C_3N_4–CPE for determination of Trp in milk (n = 5).

Sample	Spiked	Found	Recovery %
Milk	0	ND	–
	5	5.1	98
	10	9.8	102
	20	19.8	101
	30	28.5	105.2

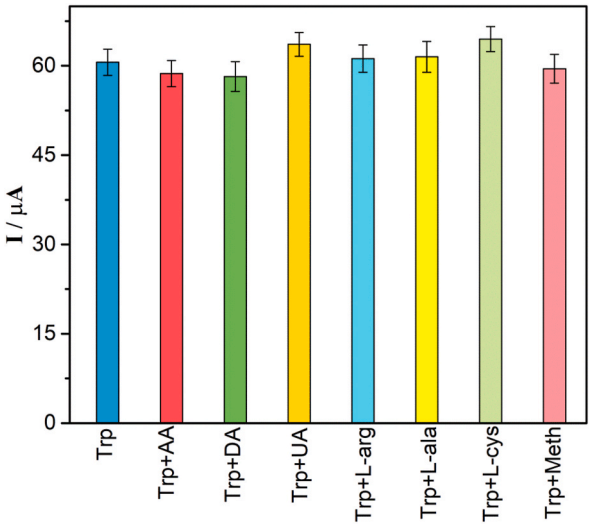

Fig. 10. Effect of Interferences on a determination of Trp at g–C_3N_4–CPE.

exhibited lower detection limit, good repeatability, reproducibility and appropriate selectivity. In addition, it was effectively employed for the detection of Trp in the milk sample.

Data availability statement

Data will be made available on request.

CRediT authorship contribution statement

Habtamu Adefris Abebe: Data curation, Formal analysis, Investigation, Methodology, Writing – original draft, Writing – review & editing. **Abebe Diro:** Investigation, Supervision, Validation. **Shimeles Addisu Kitte:** Conceptualization, Project administration, Resources, Writing – review & editing.

Declaration of competing interest

The authors declare that they have no known competing financial interests or personal relationships that could have appeared to influence the work reported in this paper.

Acknowledgements

The authors would like to acknowledge Jimma University School of Graduate Studies and Department of Chemistry for funding and material support.

References

[1] A.R. Fiorucci, É.T.G. Cavalheiro, The use of carbon paste electrode in the direct voltammetric determination of tryptophan in pharmaceutical formulations, J. Pharmaceut. Biomed. Anal. 28 (5) (2002) 909–915.
[2] S.N. Young, M. Leyton, The role of serotonin in human mood and social interaction: insight from altered tryptophan levels, Pharmacol. Biochem. Behav. 71 (4) (2002) 857–865.
[3] J.D. Schaechter, R.J. Wurtman, Serotonin release varies with brain tryptophan levels, Brain Res. 532 (1) (1990) 203–210.

[4] N.J. Benevenga, R.D. Steele, Adverse effects of excessive consumption of amino acids, Annu. Rev. Nutr. 4 (1) (1984) 157–181.
[5] M. Yamashita, T. Yamamoto, Tryptophan and kynurenic acid may produce an amplified effect in central fatigue induced by chronic sleep disorder, Int. J. Tryptophan Res. 7 (2014). IJTR.S14084.
[6] G. Ravindran, W.L. Bryden, Tryptophan determination in proteins and feedstuffs by ion exchange chromatography, Food Chem. 89 (2) (2005) 309–314.
[7] A.A. Alwarthan, Chemiluminescent determination of tryptophan in a flow injection system, Anal. Chim. Acta 317 (1) (1995) 233–237.
[8] K.D. Altria, P. Harkin, M.G. Hindson, Quantitative determination of tryptophan enantiomers by capillary electrophoresis, J. Chromatogr. B Biomed. Sci. Appl. 686 (1) (1996) 103–110.
[9] J. Ren, M. Zhao, J. Wang, C. Cui, B. Yang, Spectrophotometric method for determination of tryptophan in protein hydrolysates, Food Technol. Biotechnol. 45 (2007).
[10] J. Gautam, M. Raj, R. Goyal, Determination of tryptophan at carbon nanomaterials modified glassy carbon sensors: a comparison, J. Electrochem. Soc. 167 (2020), 066504.
[11] K.-J. Huang, C.-X. Xu, W.-Z. Xie, W. Wang, Electrochemical behavior and voltammetric determination of tryptophan based on 4-aminobenzoic acid polymer film modified glassy carbon electrode, Colloids Surf. B Biointerfaces 74 (1) (2009) 167–171.
[12] J. Zhu, P. Xiao, H. Li, S.A.C. Carabineiro, Graphitic carbon nitride: synthesis, properties, and applications in catalysis, ACS Appl. Mater. Interfaces 6 (2014) 16449–16465.
[13] L. Wang, K. Wang, T. He, Y. Zhao, H. Song, H. Wang, Graphitic carbon nitride-based photocatalytic materials: preparation strategy and application, ACS Sustain. Chem. Eng. 8 (2020) 16048–16085.
[14] R.G. Elfarargy, M.A. Saleh, M.M. Abodouh, M.A. Hamza, N.K. Allam, Graphitic carbon nitride nanoheterostructures as novel platforms for the electrochemical sensing of the chemotherapeutic and immunomodulator agent MTX, Biosensors 13 (1) (2023) 51.
[15] P. Balasubramanian, R. Settu, S.-M. Chen, T.-W. Chen, Voltammetric sensing of sulfamethoxazole using a glassy carbon electrode modified with a graphitic carbon nitride and zinc oxide nanocomposite, Microchim. Acta 185 (8) (2018) 396.
[16] J. Javanshiri-Ghasemabadi, S. Sadeghi, Facile fabrication of an electrochemical sensor for the determination of two sulfonamide antibiotics in milk, honey and water samples using the effective modification of carbon paste electrode with graphitic carbon nitride and manganese oxide nanostructures, J. Food Compos. Anal. 120 (2023), 105294.
[17] D. Ilager, N.P. Shetti, K.R. Reddy, S.M. Tuwar, T.M. Aminabhavi, Nanostructured graphitic carbon nitride (g-C3N4)-CTAB modified electrode for the highly sensitive detection of amino-triazole and linuron herbicides, Environ. Res. 204 (2022), 111856.
[18] R.N. Adams, Carbon paste electrodes, Anal. Chem. 30 (1958), 1576-1576.
[19] S.M. Ghoreishi, M. Behpour, F.S. Ghoreishi, S. Mousavi, Voltammetric determination of tryptophan in the presence of uric acid and dopamine using carbon paste electrode modified with multi-walled carbon nanotubes, Arab. J. Chem. 10 (2017) S1546–S1552.
[20] S.M. Ghoreishi, M. Behpour, N. Jafari, A. Khoobi, Determination of tyrosine in the presence of sodium dodecyl sulfate using a gold nanoparticle modified carbon paste electrode, Anal. Lett. 46 (2013) 299–311.
[21] P.-S. Ganesh, A.B. Teradale, S.-Y. Kim, H.-U. Ko, E.E. Ebenso, Electrochemical sensing of anti-inflammatory drug mesalazine in pharmaceutical samples at polymerized-Congo red modified carbon paste electrode, Chem. Phys. Lett. 806 (2022), 140043.
[22] P.-S. Ganesh, S.-Y. Kim, S. Kaya, R. Salim, An experimental and theoretical approach to electrochemical sensing of environmentally hazardous dihydroxy benzene isomers at polysorbate modified carbon paste electrode, Sci. Rep. 12 (1) (2022) 2149.
[23] J. Tashkhourian, M.R.H. Nezhad, J. Khodavesi, S. Javadi, Silver nanoparticles modified carbon nanotube paste electrode for simultaneous determination of dopamine and ascorbic acid, J. Electroanal. Chem. 633 (2009) 85–91.
[24] J. Estrada-Aldrete, J.M. Hernández-López, A.M. García-León, J.M. Peralta-Hernández, F.J. Cerino-Córdova, Electroanalytical determination of heavy metals in aqueous solutions by using a carbon paste electrode modified with spent coffee grounds, J. Electroanal. Chem. 857 (2020), 113663.
[25] B. Niu, B. Yao, M. Zhu, H. Guo, S. Ying, Z. Chen, Carbon paste electrode modified with fern leave-like MIL-47(as) for electrochemical simultaneous detection of Pb(II), Cu(II) and Hg(II), J. Electroanal. Chem. 886 (2021), 115121.
[26] N.B. Ashoka, B.E.K. Swamy, H. Jayadevappa, S.C. Sharma, Simultaneous electroanalysis of dopamine, paracetamol and folic acid using TiO2-WO3 nanoparticle modified carbon paste electrode, J. Electroanal. Chem. 859 (2020), 113819.
[27] S. Deepa, B.E.K. Swamy, K.V. Pai, A surfactant SDS modified carbon paste electrode as an enhanced and effective electrochemical sensor for the determination of doxorubicin and dacarbazine its applications: a voltammetric study, J. Electroanal. Chem. 879 (2020), 114748.
[28] J. Penagos-Llanos, O. García-Beltrán, J.A. Calderón, J.J. Hurtado-Murillo, E. Nagles, J.J. Hurtado, Simultaneous determination of tartrazine, sunset yellow and allura red in foods using a new cobalt-decorated carbon paste electrode, J. Electroanal. Chem. 852 (2019), 113517.
[29] F. Melak, M. Redi, M. Tessema, E. Alemayehu, Electrochemical determination of catechol in tea samples using anthraquinone modified carbon paste electrode, Nat. Sci. 5 (2013) 888–894.
[30] X. Wang, K. Maeda, A. Thomas, K. Takanabe, G. Xin, J.M. Carlsson, K. Domen, M. Antonietti, A metal-free polymeric photocatalyst for hydrogen production from water under visible light, Nat. Mater. 8 (1) (2009) 76–80.
[31] D. Liu, Z. Zhang, F. Luo, J. Wu, Elemental mercury capture from simulated flue gas by graphite-phase carbon nitride, Energy & Fuels 34 (6) (2020) 6851–6861.
[32] H.-B. Fang, Y. Luo, Y.-Z. Zheng, W. Ma, X. Tao, Facile large-scale synthesis of urea-derived porous graphitic carbon nitride with extraordinary visible-light spectrum photodegradation, Ind. Eng. Chem. Res. 55 (16) (2016) 4506–4514.
[33] J. Xu, Y. Li, S. Peng, G. Lu, S. Li, Eosin Y-sensitized graphitic carbon nitride fabricated by heating urea for visible light photocatalytic hydrogen evolution: the effect of the pyrolysis temperature of urea, Phys. Chem. Chem. Phys. 15 (20) (2013) 7657–7665.
[34] Q. He, Y. Tian, Y. Wu, J. Liu, G. Li, P. Deng, D. Chen, Electrochemical sensor for rapid and sensitive detection of tryptophan by a Cu2O nanoparticles-coated reduced graphene oxide nanocomposite, Biomolecules 9 (5) (2019) 176.
[35] P. Chamorro-Posada, R.C. Dante, J. Vázquez-Cabo, D.G. Dante, P. Martín-Ramos, Ó. Rubiños-López, F.M. Sánchez-Arévalo, From urea to melamine cyanurate: study of a class of thermal condensation routes for the preparation of graphitic carbon nitride, J. Solid State Chem. 310 (2022), 123071.
[36] C. Li, X. Yang, B. Yang, Y. Yan, Y. Qian, Synthesis and characterization of nitrogen-rich graphitic carbon nitride, Mater. Chem. Phys. 103 (2) (2007) 427–432.
[37] D.R. Paul, R. Sharma, S.P. Nehra, A. Sharma, Effect of calcination temperature, pH and catalyst loading on photodegradation efficiency of urea derived graphitic carbon nitride towards methylene blue dye solution, RSC Adv. 9 (27) (2019) 15381–15391.
[38] J. Zhu, P. Xiao, H. Li, S.A.C. Carabineiro, Graphitic carbon nitride: synthesis, properties, and applications in catalysis, ACS Appl. Mater. Interfaces 6 (19) (2014) 16449–16465.
[39] H.S. Magar, R.Y.A. Hassan, A. Mulchandani, Electrochemical impedance spectroscopy (EIS): principles, construction, and biosensing applications, Sensors 21 (19) (2021).
[40] F.A. Bushira, S.A. Kitte, Y. Wang, H. Li, P. Wang, Y. Jin, Plasmon-boosted Cu-doped TiO2 oxygen vacancy-rich luminol electrochemiluminescence for highly sensitive detection of alkaline phosphatase, Anal. Chem. 93 (45) (2021) 15183–15191.
[41] R. Sundaresan, V. Mariyappan, S.-M. Chen, M. Keerthi, R. Ramachandran, Electrochemical sensor for detection of tryptophan in the milk sample based on MnWO4 nanoplates encapsulated RGO nanocomposite, Colloids Surf. A Physicochem. Eng. Asp. 625 (2021), 126889.
[42] H. Beitollahi, F. Garkani-Nejad, S. Tajik, M.R. Ganjali, Voltammetric determination of acetaminophen and tryptophan using a graphite screen printed electrode modified with functionalized graphene oxide nanosheets within a $Fe_{(3)}O_{(4)}$@$SiO_{(2)}$ nanocomposite, Iran. J. Pharm. Res. (IJPR) 18 (1) (2019) 80–90.
[43] S. Manavalan, J. Ganesamurthi, S.-M. Chen, P. Veerakumar, K. Murugan, A robust Mn@FeNi-S/graphene oxide nanocomposite as a high-efficiency catalyst for the non-enzymatic electrochemical detection of hydrogen peroxide, Nanoscale 12 (10) (2020) 5961–5972.
[44] C. Rajkumar, B. Thirumalraj, S.-M. Chen, P. Veerakumar, S.-B. Liu, Ruthenium nanoparticles decorated tungsten oxide as a bifunctional catalyst for electrocatalytic and catalytic applications, ACS Appl. Mater. Interfaces 9 (37) (2017) 31794–31805.
[45] N.S. Prinith, J.G. Manjunatha, Electrochemical analysis of L-Tryptophan at highly sensitive poly(Glycine) modified carbon nanotube paste sensor, Mater. Res. Innovat. 26 (3) (2022) 134–143.

[46] Y. Zhang, G.I.N. Waterhouse, Z.-p. Xiang, J. Che, C. Chen, W. Sun, A highly sensitive electrochemical sensor containing nitrogen-doped ordered mesoporous carbon (NOMC) for voltammetric determination of l-tryptophan, Food Chem. 326 (2020), 126976.
[47] J. Han, J. Zhao, Z. Li, H. Zhang, Y. Yan, D. Cao, G. Wang, Nanoporous carbon derived from dandelion pappus as an enhanced electrode material with low cost for amperometric detection of tryptophan, J. Electroanal. Chem. 818 (2018) 149–156.
[48] D. Sun, H. Li, M. Li, C. Li, H. Dai, D. Sun, B. Yang, Electrodeposition synthesis of a NiO/CNT/PEDOT composite for simultaneous detection of dopamine, serotonin, and tryptophan, Sensor. Actuator. B Chem. 259 (2018) 433–442.
[49] F. Rezaei, N. Ashraf, G.H. Zohuri, A smart electrochemical sensor based upon hydrophilic core–shell molecularly imprinted polymer for determination of L-tryptophan, Microchem. J. 185 (2023), 108260.
[50] S. Zhang, P. Ling, Y. Chen, J. Liu, C. Yang, 2D/2D porous Co_3O_4/rGO nanosheets act as an electrochemical sensor for voltammetric tryptophan detection, Diam. Relat. Mater. 135 (2023), 109811.
[51] Ž.Z. Tasić, M.B.P. Mihajlović, M.B. Radovanović, A.T. Simonović, D.V. Medić, M.M. Antonijević, Electrochemical determination of L-tryptophan in food samples on graphite electrode prepared from waste batteries, Sci. Rep. 12 (1) (2022) 5469.
[52] Y. Haldorai, S.-H. Yeon, Y.S. Huh, Y.-K. Han, Electrochemical determination of tryptophan using a glassy carbon electrode modified with flower-like structured nanocomposite consisting of reduced graphene oxide and SnO2, Sensor. Actuator. B Chem. 239 (2017) 1221–1230.
[53] F. Pogacean, C. Varodi, M. Coros, I. Kacso, T. Radu, B.I. Cozar, V. Mirel, S. Pruneanu, Investigation of L-tryptophan electrochemical oxidation with a graphene-modified electrode, Biosensors 11 (2) (2021) 36.